ISSN 2070-0482, Mathematical Models and Computer Simulations, 2016, Vol. 8, No. 5, pp. 523–532. © Pleiades Publishing, Ltd., 2016.
Original Russian Text © N.G. Burago, A.B. Zhuravlev, I.S. Nikitin, V.L. Yakushev, 2016, published in Matematicheskoe Modelirovanie, 2016, Vol. 28, No. 2, pp. 53–64.

A Study of Different Modes of Fatigue Fracture and Durability Estimation for Compressor Disks of Gas-Turbine Engines

N. G. Burago[a], A. B. Zhuravlev[a], I. S. Nikitin[b,*], and V. L. Yakushev[b]

[a] *Ishlinsky Institute for Problems in Mechanics, Russian Academy of Sciences, Moscow, Russia*

[b] *Institute for Computer-Aided Design, Russian Academy of Sciences, Moscow, Russia*

**e-mail: i_nikitin@list.ru*

Received June 29, 2015

Abstract—Various criteria of multiaxial fatigue fracture are studied for low-cycle fatigue (LCF); their generalizations are proposed for a very-high-cycle fatigue (VHCF) regime. The procedure of the stress state calculation is described for the compressor disk of the gas-turbine engine (GTE) in the flight cycle of loading and for the low-amplitude vibrations of the blades. The durability estimations of the disk operation are obtained for alternative mechanisms of LCF and VHCF using the calculated stress state and the models of multiaxial fatigue fracture. The results are compared with the data observed during operations.

Keywords: low-cycle fatigue, very-high-cycle fatigue, durability estimation, stress concentration, centrifugal loading, high-frequency vibrations

DOI: 10.1134/S2070048216050070

1. INRODUCTION

Currently, there are several main types of criteria and models of fatigue fracture, allowing us to estimate the number of loading cycles for a material sample (construction element) until its fracture with respect to its stress state, strain state, or fatigue accumulation (see [1–10]). It is not easy to determine the parameters of the considered models: it is an experimental task using results of uniaxial fatigue extension, torsion, or bending tests with various asymmetry coefficients of the cycle.

In the present paper, we describe principal criteria of multiaxial fatigue fracture with respect to its stress state under the conditions of low-cycle fatigue (LCF, see [2, 3, 11–13]), propose their generalizations for the case of very-high-cycle fatigue (VHCF), and apply them to estimate the durability of the elements of a sample technical construction.

Note that, during a multiyear exploitation, constructions work within the elasticity limits and plastic effects are not observed until the fracture starts. Therefore, to compute the durability according to the criteria of fatigue fracture, it suffices to solve the corresponding problem of elasticity theory and find the variation limits of the stress-strain state of the disk in the cyclic process. Once macrofailures such as fatigue cracks appear and irreversible deformations begin to develop, the remaining lifetime of the construction is negligible compared to the full operating time. That is why we do not consider studying the dependence of the growth of fatigue cracks on the number of loading cycles and the form of the stressed state in the present paper.

In [15, 16], durability estimates are obtained for varying-width disks (compressor disks of gas-turbine engines) in flight loading cycles of the kind "takeoff–flight–landing" under centrifugal loads and aerodynamic pressures applied to blades. This cyclic process corresponds to the low-cycle fatigue (LCF) regime. However, in recent years, much attention is paid to the study of the very-high-cycle fatigue (VHCF) related to long-term high-frequency oscillations of structural elements (see [1]). In particular, processes of this kind in compressor disks of gas-turbine engines are caused by blade oscillations. Their frequency is of the same order as the rotation frequency of the disk or is a multiple for it. If a VHCF develops to N exceeding 10^8 (where N is the number of cycles to fracture), then fatigue focuses might appear in the neighborhoods of the contact zones between the blades and the disk.

Thus, apart from LCF flight loadings, constructions undergo low-amplitude vibration VHCF loadings. Long-term vibrations might also destroy the constructions. Note that, under long-term exploitation,

the stress amplitude in the disks is substantially lower than the yield limit. According to the classical approaches, the work of disks within the elasticity limits is completely safe. However, in long-term exploitation, fatigue damage occurs even when the structure works within the elasticity limits up to appearance of damage. Fractography of the fracture surfaces shows that fatigue damage might occur in both LCF and VHCF modes. A distinctive feature of damage in VHCF mode is that the zone of damage is under the surface of the structural element, and not adjacent to it, as in the case of LCF regime. These features allow experimenters to distinguish between these mechanisms in the classification of the primary damage mode. Remark that further development of fatigue cracks typically occurs in an accelerated LCF mode and is observed as set of fatigue grooves on the fracture surface. This implies that these fatigue fracture regimes are alternative to each other and they frequently complement and strengthen each other. Reviews of the experimental investigations in these directions can be found in [1, 14].

Remark that in LCF mode, disk is under action of centrifugal forces and contact forces between disk and blades that are additionally loaded by the aerodynamic pressure. In VHCF mode, additional loads are caused by the action of torsional vibrations of the blades. Here we do not consider the reasons for blade vibrations such as pressure pulsation, excitation of own forms vibrations, influence of transient engine operation modes. The frequencies and amplitudes of the vibrations are assumed to be given according [1].

Since the problem of elasticity theory is linear, it follows that the stress-strain states (SSS) caused by the flight cycles (LCF) and due to vibrations (VHCF) can be computed separately and then the full SSS may be obtained by summing. The full stress-strain states, calculated for two extreme vibrating blade positions, are the boundaries of the studied cyclic process. These SSS are used in the criteria of fatigue fracture. By using the multi-axial criteria of fatigue fracture, we find the spatial distribution of safe exploitation time and position of fatigue damage zones.

Currently, no theoretical and experimentally justified criteria exist for detection of safe exploitation time in the VHCF processes. Therefore, to estimate such time for vibrating structure elements, we use generalization [11–13] of known multiaxial criteria for the LCF mode ($N < 10^5$) onto VHCF mode ($N > 10^8$).

As an example, we have calculated time up to appearance the fatigue damage for disk of the compressor (gas-turbine engine GTE D30). Firstly, we have calculated the stress-strain state of the contact system of disk and blades in LCF and VHCF modes. Then we have used the computed stresses and strains in various fatigue fracture criteria in order to obtain durability estimates of the typical disk under exploitation conditions in the cases of two alternative fatigue damage modes.

2. MULTIAXIAL FATIGUE-FRACTURE MODELS FOR THE VHCF REGIME

2.1. Models of Estimates with Respect to the Stress State

To find the parameters of the models of multiaxial fatigue fracture, we use the experimental curves of uniaxial cyclic tests for various values of the asymmetry parameter $R = \sigma_{\min}/\sigma_{\max}$ of the cycle, where $\sigma_{\max}$ and $\sigma_{\min}$ are the greatest and least values of the stress in the cycle. Describing the uniaxial fatigue fracture test results, we use the following notation: $\sigma_a = (\sigma_{\max v} - v\sigma_{\min})/2$ is the stress amplitude in the cycle and $\Delta\sigma = \sigma_{\max} - \sigma_{\min}$ is the stress range in the uniaxial loading cycle.

The experimental data of the uniaxial tests are described by the Wohler curves analytically represented by Basquin formula [2, 3]

$$\sigma = \sigma_u + \sigma_c N^{\beta}, \tag{1}$$

where σ_u is the fatigue limit, σ_c is the fatigue strength factor, β is the fatigue strength exponent, and N is the number of cycles to fracture. The general form of the fatigue curve is represented in Fig. 1; for LCF mode the left-hand branch of the curve (for $N < 10^7$) is of interest.

The fatigue fracture investigation problem is as follows: to find the spatial distribution of the number of cycles to fracture N from equations (1), generalized for multiaxial stress state, using computed stresses in structure under consideration. Consider generalizations [2] of uniaxial fatigue tests to multiaxial stress state.

2.1.1. The Sines model. Due to [11], the uniaxial fatigue curve represented by Eq. (1) is generalized to the multiaxial stress state as follows:

$$\begin{gathered}\Delta\tau/2 + \alpha_s\sigma_{\text{mean}} = S_0 + AN^{\beta}, \quad \sigma_{\text{mean}} = (\sigma_1 + \sigma_2 + \sigma_3)_{\text{mean}}, \\ \Delta\tau = \sqrt{(\Delta\sigma_1 - \Delta\sigma_2)^2 + (\Delta\sigma_1 - \Delta\sigma_3)^2 + (\Delta\sigma_2 - \Delta\sigma_3)^2}\big/3,\end{gathered} \tag{2}$$

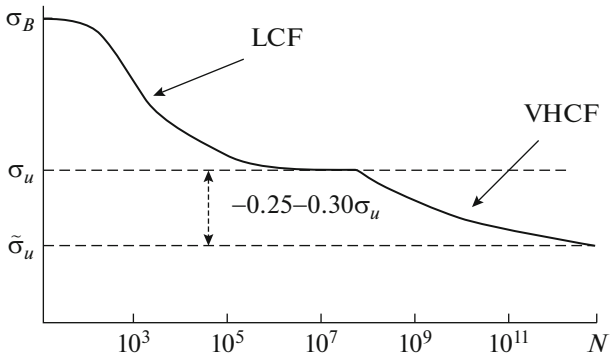

Fig. 1. The bimodal fatigue curve.

where σ_{mean} is the sum of principal stresses averaged over the loading cycle; $\Delta\tau$ is the variation of the octahedral tangential stress over the cycle; $\Delta\tau/2$ is its amplitude; and α_s, S_0, A, and β are the parameters determined according to the experimental data.

The model parameters determined by means of the uniaxial fatigue curves at $R = -1$ and $R = 0$ are found in [2]:

$$S_0 = \sqrt{2}\sigma_u/3, \quad A = 10^{-3\beta}\sqrt{2}(\sigma_B - \sigma_u)/3, \quad \alpha_s = \sqrt{2}(2k_{-1} - 1)/3, \text{ and } k_{-1} = \sigma_u/(2\sigma_{u0}), \tag{3}$$

where σ_u and σ_{u0} are the fatigue limits on curves $\sigma_a(N)$ at $R = -1$ and $R = 0$ respectively.

2.1.2. The Crossland model. Due to [12], the uniaxial fatigue curve is generalized to the multiaxial stress state as follows:

$$\Delta\tau/2 + \alpha_c(\overline{\sigma}_{\max} - \Delta\tau/2) = S_0 + AN^{\beta}, \quad \overline{\sigma}_{\max} = (\sigma_1 + \sigma_2 + \sigma_3)_{\max}, \tag{4}$$

where $\overline{\sigma}_{\max}$ is the greatest (over the loading cycle) sum of principal stresses, while α_c, S_0, A, and β are the parameters to be determined.

In this case, the model parameters are equal to

$$\begin{gathered} S_0 = \sigma_u\left[\sqrt{2}/3 + (1 - \sqrt{2}/3)\alpha_c\right], \quad A = 10^{-3\beta}\left[\sqrt{2}/3 + (1 - \sqrt{2}/3)\alpha_c\right](\sigma_B - \sigma_u), \\ \alpha_c = (k_{-1}\sqrt{2}/3 - \sqrt{2}/6)\Big/\left[(1 - \sqrt{2}/6) - k_{-1}(1 - \sqrt{2}/3)\right] \end{gathered} \tag{5}$$

(see [2]).

2.1.3. The Findley model. Due to [13], the uniaxial fatigue curve is generalized to the multiaxial stressed state as follows:

$$(\Delta\tau_s/2 + \alpha_F\sigma_n)_{\max} = S_0 + AN^{\beta}, \tag{6}$$

where τ_s and σ_n are the absolute magnitudes of tangent stress and normal stress for the plane with normal vector n_i, the subscript max denotes that for this plane the combination $\Delta\tau_s/2 + \alpha_F\sigma_n$ takes the greatest value, while α_F, S_0, A, and β are determined by means of uniaxial fatigue curves at $R = -1$ and $R = 0$:

$$\begin{gathered} S_0 = \sigma_u\left(\sqrt{1 + \alpha_F^2} + \alpha_F\right)\Big/2, \quad A = 10^{-3\beta}(\sqrt{1 + \alpha_F^2} + \alpha_F)(\sigma_B - \sigma_u)/2, \\ \alpha_F = \frac{\sqrt{5k_{-1}^2 - 2k_{-1}}/2 - k_{-1}(1 - k_{-1})}{k_{-1}(2 - k_{-1})}. \end{gathered} \tag{7}$$

In presented below example the following approximate parameters for titanium alloy Ti-6Al-4V [8] are used. Strength limit: $\sigma_B = 1100$ MPa fatigue limits along fatigue curves at $R = -1$ and $R = 0$, respecively:

σ_u = 450 MPa and σ_{u0} = 350 MPa, exponent factor in the power-law dependence of fatigue limit on the number of cycles to fracture: $\beta = -0.45$, Young's modulus: E = 116 GPa, shear modulus: G = 44 GPa Poisson's ratio: $\nu = 0.32$.

3. THE LCF FLIGHT LOADING CYCLE: AN EXAMPLE OF THE COMPUTATION OF THE MULTIAXIAL STRESS STATE AND THE DURABILITY ESTIMATE FOR STRUCTURE ELEMENTS

3.1. The Compressor Disk: a Computational Model

As an example, consider the problem of fatigue failure of the compressor disk of gas turbine engine in flight cycles of loading (low-cycle fatigue mode). Assume that the multiaxial loading cycle for the system "disk–blade" is the flight loading cycle (FLC) such that the aircraft achieves the greatest loading at the cruising flight speed and the corresponding angular velocities of the compressor disk rotation. We have to determine spatial distribution of N (number of FLC to fracture) using relations (2), (4), and (6). To do that, one has to compute the SSS for the disk–blade system loaded by the centrifugal forces, distributed aerodynamic pressures, and the forces of nonlinear contact interactions between the disk, blades, and additional construction elements (see below).

The SSS of the contact disk–blade system is determined by the system of equations

$$\rho d\mathbf{v}/dt = \nabla\cdot\boldsymbol{\sigma} + \rho g, \quad d\boldsymbol{\sigma}/dt = \lambda(\mathbf{e}:\mathbf{I})\mathbf{I} + 2\mu\mathbf{e}, \quad e = (\nabla\mathbf{v} + \nabla\mathbf{v}^{\mathrm{T}})/2, \quad d\mathbf{u}/dt = \mathbf{v},$$

including motion equations, the Hooke elasticity law differentiated with respect to time, and the kinematic relationships between strain rate tensor $\mathbf{e}$, displacement $\mathbf{u}$ and velocity $\mathbf{v}$. Here $\mathbf{I}$ is the unit tensor, λ and μ are the Lame elasticity constants, $\boldsymbol{\sigma}$ is the Cauchy stress tensor, $\rho\mathbf{g}$ is the centrifugal force, ρ is the density, and the superscript "T" denotes the transposition operation.

Boundary of solution region V consists of three parts of different types: $S = S_p \cup S_v \cup S_c$; the external loadings, velocities, and contact conditions are set on each part (respectively). For S_p and S_v, the conditions have the form

$$t \ge 0, \quad \mathbf{x}\in S_p: \quad \sigma_n = (\boldsymbol{\sigma}\cdot\mathbf{n})\cdot\mathbf{n} = p_n^*, \quad \sigma_{n\alpha} = (\boldsymbol{\sigma}\cdot\mathbf{n})\cdot\boldsymbol{\tau}_\alpha = T_\alpha^*,$$

$$t \ge 0, \quad \mathbf{x}\in S_v: \quad \mathbf{v} = \mathbf{v}_*,$$

where $\mathbf{x}$ is a boundary point, $\mathbf{n}$ and $\boldsymbol{\tau}_\alpha$ ($\alpha = 1, 2$) are the unit normal and tangential vectors to the boundary, and p_n^* is the aerodynamic pressure; the starred values are assumed to be given. For surface aerodynamic loading, we have $T_\alpha^* = 0$.

The contact conditions of various types are set on contact surfaces S_c; to denote them, we use the notation $[v_{\tau\alpha}]$ ($\alpha = 1, 2$) and $[u_n]$ for jumps of the tangential velocities and normal displacements, respectively. It is assumed that the normal and tangential stresses are continuous on the contact boundaries, i.e., $[\sigma_n] = [\sigma_{n\alpha}] = 0$, and the friction coefficient q is nonnegative and does not depend on the tangent direction.

The following types of contact conditions are considered ($t \ge 0$):

—the frictional contact:

$$\mathbf{x}\in S_c: \quad \sigma_n < 0, \quad |\sigma_{n\alpha}| < q|\sigma_n|, \quad [\mathbf{v}_{\tau\alpha}] = 0, \quad \text{and} \quad [u_n] = 0 \ \text{ for the friction of rest}$$

and

$$\mathbf{x}\in S_c: \quad \sigma_n < 0, \quad \sigma_{n\alpha} = q|\sigma_n|[\mathbf{v}_{\tau\alpha}]/|[\mathbf{v}_{\tau\alpha}]|, \quad [\mathbf{v}_{\tau\alpha}] \ne 0, \quad \text{and} \quad [u_n] = 0 \text{ for the sliding friction}$$

(here $\alpha = 1, 2$ and, if $q = 0$, then the frictionless sliding or smooth contact takes place);

—the detachment: $\mathbf{x}\in S_c$: $[u_n] \ge 0$, $\sigma_{n\alpha} = \sigma_n = 0$ ($\alpha = 1, 2$);

—the complete sticking (ideal contact): $\mathbf{x}\in S_c$: $[\mathbf{u}] = [\sigma_n] = [\sigma_{n\alpha}] = 0$ ($\alpha = 1, 2$).

The initial value conditions are as follows: $t = 0$, $\mathbf{x}\in V$: $\mathbf{u} = 0$, $\mathbf{v} = 0$, $\boldsymbol{\sigma} = 0$.

To analyze the three-dimensional stress-strain state of the contact system of disk and blades we used finite element method. The distribution of aerodynamic pressure was found analytically by methods of complex variable theory using the hypothesis of isolated profile and the classical solutions of the flow problem for a lattice of plates under arbitrary angle of attack. The deformation of blades was taken into account (details see in [15, 18, 19]).

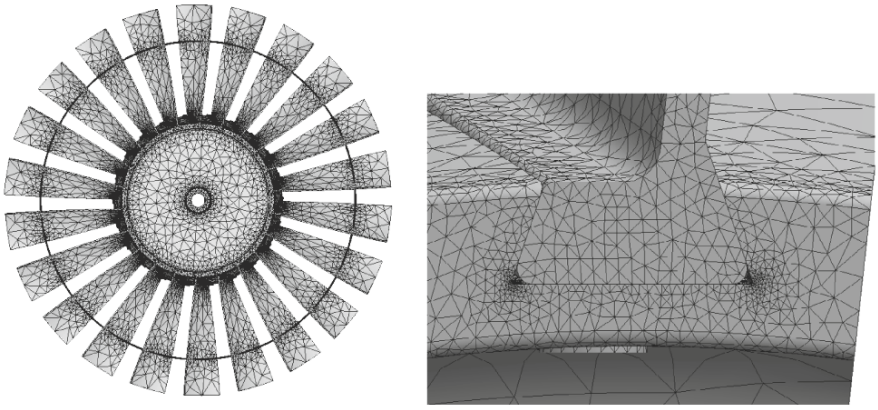

Fig. 2. (a) The full geometric finite-element model. (b) The computational grid for the sector.

The stress concentration in the vicinity of the contact boundary of dovetail type leads to a need for a significant refinement of the computational grid in this area. Estimates show that the full-scale calculation model for disk with a full set of the blades and with a sufficient number of finite elements requires too many computer time and memory. In the same time, it is more economical to calculate a single sector of the disk with single blade using sufficient finite element grid. But in this case boundary conditions at lateral surfaces remain unknown. That is why, the calculation was carried out in two stages. In the first stage a full-scale model (Fig. 2) has been calculated on a coarse grid with the number of elements of approximately 2×10^5. In the second stage a separate sector of the disk with a single blade has been calculated on a fine grid. At the lateral surfaces, the displacements had the values obtained from the calculation of a full-scale model.

The finite element grid for the computation of single sector with a blade is displayed in Fig. 2b. The grid is substantially condensed in vicinity of the expected stress concentrators. The full number of elements does not exceed 100000, which is acceptable for a personal computer computation.

The following computation parameters were assigned: the angular rotation velocity ω is 314 rad/s (3000 rpm) and the velocity head at infinity $\rho v_\infty^2/2$ is 26000 N/m^2, which corresponds to the flow velocity of 200 m/s with density 1.3 kg/m^3. The following material properties were assigned: for the disk (of the titanium alloy), $E = 116$ GPa, $\nu = 0.32$, and $\rho = 4370$ kg/m^3; for the blades (of an aluminum alloy), $E = 69$ GPa, $\nu = 0.33$, and $\rho = 2700$ kg/m^3; and for fixing pins (the steel), $E = 207$ GPa, $\nu = 0.27$, and $\rho = 7860$ kg/m^3.

Our computations indicate that contact zones of dovetail type between disk and blades are the most dangerous with respect to appearance of the fatigue cracks. Detachment and slippage with friction at the contact boundaries should be taken into account for best concordance between calculated and observed locations of stress concentration zones. For technological reasons, the complete sticking is set at the boundary of fixing pin (see Fig. 3a). In Fig. 3b, the zone of maximal tensile stresses is located at the left corner of the blade groove. To display the stress value, 12 shades of gray are used for the range between 0 and 240 MPa. It is seen that the stress concentration is increasing from the front part of the groove to its back part. This matches the observation data about location of fatigue cracks at the back part of the groove (see [1]).

3.2. Durability Estimates According to the LCF Criteria

The minimum durability is observed in vicinity of left corner of the contact joint of dovetail type for disc and blade in the areas of maximum stress concentration that shown in Fig. 4 by solid lines. Fig.4b shows the calculated value of the number of flight cycles to fracture N for the selected multiaxial criteria and models of fatigue fracture. The horizontal axis corresponds to dimensionless coordinate along left corner rounding of the groove. The vertical axis corresponds to dimensionless coordinate along the groove axis.

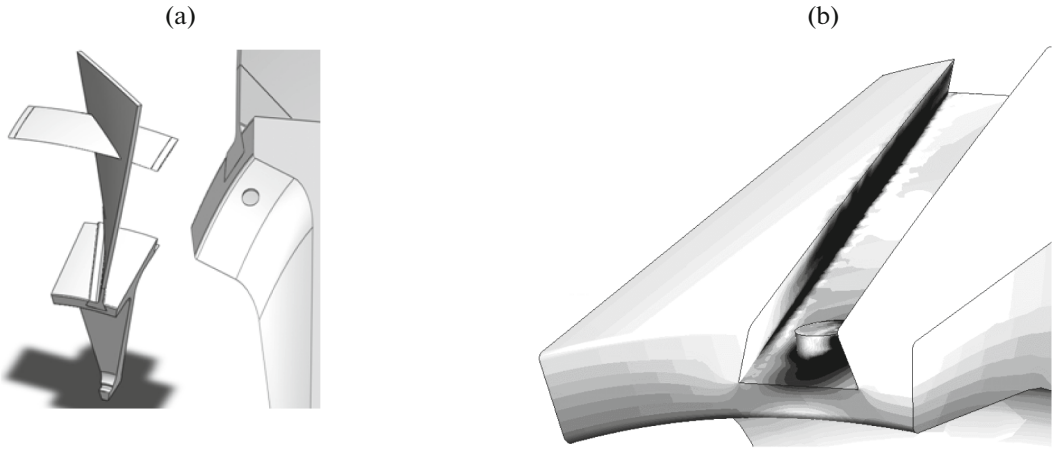

Fig. 3. (a) The disk sector with blade. (b) The greatest principal stress.

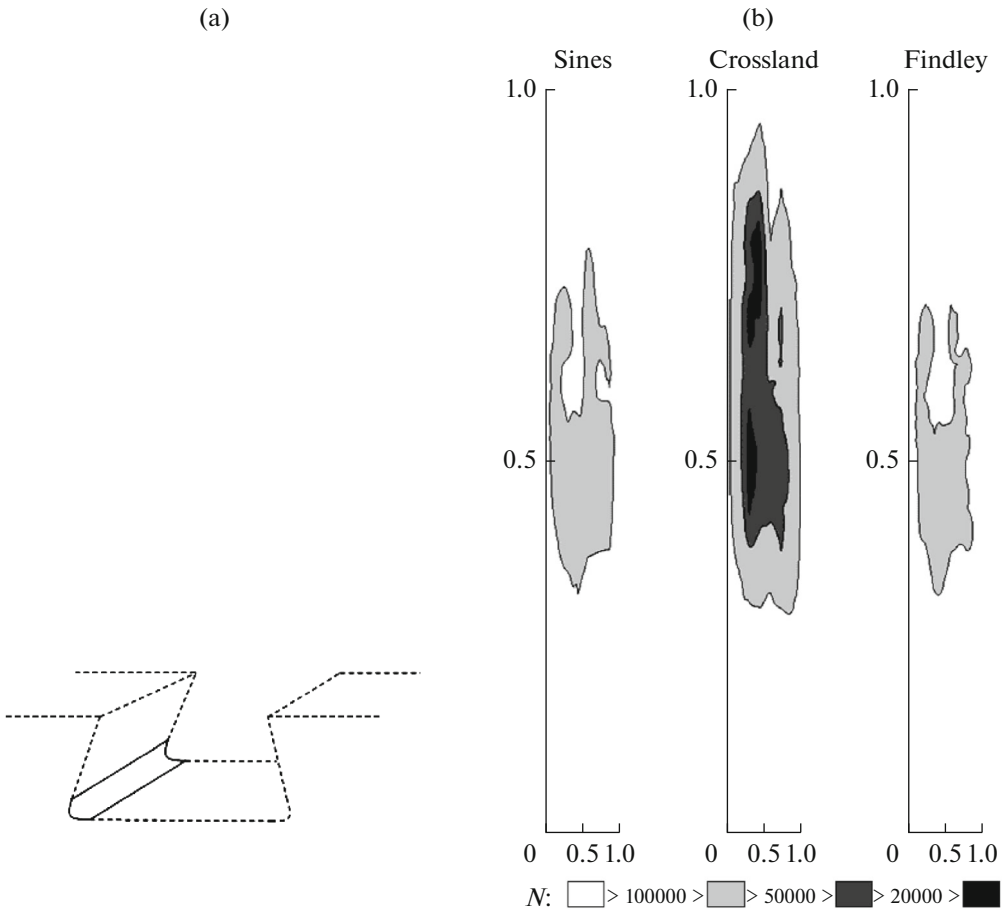

Fig. 4. (a) The zone of stress concentration. (b) The durability distribution for LCF.

The results of calculation SSS and estimates of the number of flight cycles to fracture N have been compared with the observation results [1] regarding the regularities in the appearance and growth of fatigue cracks.

Sines and Findlay criteria evaluated the durability of turbine engine disks at 20000–50000 flight cycles. Crossland criterion predicted the possibility of fatigue fracture after less than 20000 flight cycles. In general, all these criteria point to the one and the same location of expected fatigue fracture zone.

4. MULTIAXIAL STRESS STATES AND DURABILITY ESTIMATES FOR THE GTE COMPRESSOR DISK UNDER HIGH-FREQUENCY OSCILLATIONS: A COMPUTATIONAL EXAMPLE

4.1. Fatigue Fracture: an Aternative Mechanism. Multiaxial Criteria for VHCF

Additionally, we investigate an alternative fatigue fracture mechanism related to the observed high-frequency oscillations of the shroud ring. The amplitudes of these oscillations and perturbations of the stressed state caused by these oscillations in the neighborhood of the stress concentrator are relatively small, but the number of high-frequency cycles might achieve values of 10^9–10^{10} (during the exploitation period). This means that it is necessary to investigate the VHCF regime and fatigue fracture possibilities at stress levels below the classical fatigue limit of the material (see [1, 14]).

Currently, no models of multiaxial fatigue are experimentally justified for the VHCF regime. Therefore, to estimate the durability, we adapt the known criteria (2), (4), and (6) of the multiaxial LCF regime to the VHCF regime, taking into account the similarity of the left-hand and right-hand branches of the fatigue curves corresponding to the LCF regime and VHCF regime respectively (see Fig. 1).

4.1.1. Generalization of the Sines model (Eq. 2). To find parameters of the multiaxial model, we take the uniaxial fatigue curves in the VHCF regime and use the same reasoning as in the LCF regime above. To take into account the similarity of the left-hand and right-hand branches of the fatigue curve, we use the substitutions $\sigma_B \to \sigma_u$, $\sigma_u \to \tilde{\sigma}_u$, and $\sigma_{u0} \to \tilde{\sigma}_{u0}$, where $\tilde{\sigma}_u$ and $\tilde{\sigma}_{u0}$ are the new fatigue limits in the right-hand branch of the fatigue curve for the asymmetry coefficients $R = -1$ and $R = 0$. For the Sines model generalized for the VHCF regime (Eq. 3), the values of the parameters are as follows:

$$S_0 = \sqrt{2}\tilde{\sigma}_u/3, \quad A = 10^{-8\beta}\sqrt{2}(\sigma_u - \tilde{\sigma}_u)/3, \quad \alpha_s = \sqrt{2}(2k_{-1} - 1)/3, \text{ and } k_{-1} = \tilde{\sigma}_u/\tilde{\sigma}_{u0}/2.$$

4.1.2. Generalization of the Crossland model (Eq. 4). In the same way, for the Crossland model generalized for the VHCF regime (Eq. 5), the values of the parameters are as follows:

$$S_0 = \tilde{\sigma}_u\left[\sqrt{2}/3 + (1 - \sqrt{2}/3)\alpha_c\right] \text{ and } A = 10^{-8\beta}(\sigma_u - \tilde{\sigma}_u)\left[\sqrt{2}/3 + (1 - \sqrt{2}/3)\alpha_c\right].$$

4.1.3. Generalization of the Findley model (Eq. 6). In the same way, we find the values of the parameters for the Findley model generalized for the VHCF regime:

$$S_0 = \tilde{\sigma}_u\left(\sqrt{1 + \alpha_F^2} + \alpha_F\right)/2 \text{ and } A = 10^{-8\beta}(\sigma_u - \tilde{\sigma}_u)(\sqrt{1 + \alpha_F^2} + \alpha_F/2).$$

The following values of the fatigue parameters of the titanium alloy are selected for the computation in the VHCF regime: $\sigma_u = 450$ MPa, $\tilde{\sigma}_u = 250$ MPa, $\tilde{\sigma}_{u0} = 200$ MPa, and $\beta = -0.3$.

4.2. Computations of the Low-Amplitude Axial Oscillations of the Shroud Ring

The axial displacements of the shroud flanges are related to the wave perturbations propagated along the angular coordinate. Usually, from 12 to 16 half-waves cover the full set of blades. Thus, two positions of a one-blade sector of the disk can be introduced as extreme states of the basic cycle for this loading type. For those positions, the axial displacements of the left-hand endpoint of a shroud ring are directed opposite to each other provided that its left-hand endpoint is not displaced; in the exploitation regimes, the axial displacements of the left-hand endpoint achieve 1 mm. The considered low-amplitude vibrations are superimposed on the main stressed state in the flight loading cycle, determined by the cruising speed and the base frequency of the disk rotation computed in Sec. 3.

In Fig. 5a, the application scheme of the low-amplitude axial displacements is displayed. Thus, we consider the cases where the maximum or minimum of the oscillation amplitude (it is equal to ± 1 mm for the frequency of 3000 rpm) takes place on the left-hand boundary. In Fig. 5b, we display the distribution of the greatest principal stress in the groove area at the greatest angle of the blade twisting in the high-frequency cycle of its rotating oscillations; both centrifugal and aerodynamic disk loadings are taken into account. To display the stress value, 12 shades of gray are used for the range between 0 and 240 MPa. We see that, as in the LCF case, the zone of the stress concentration is located at the left-hand angle of the groove.

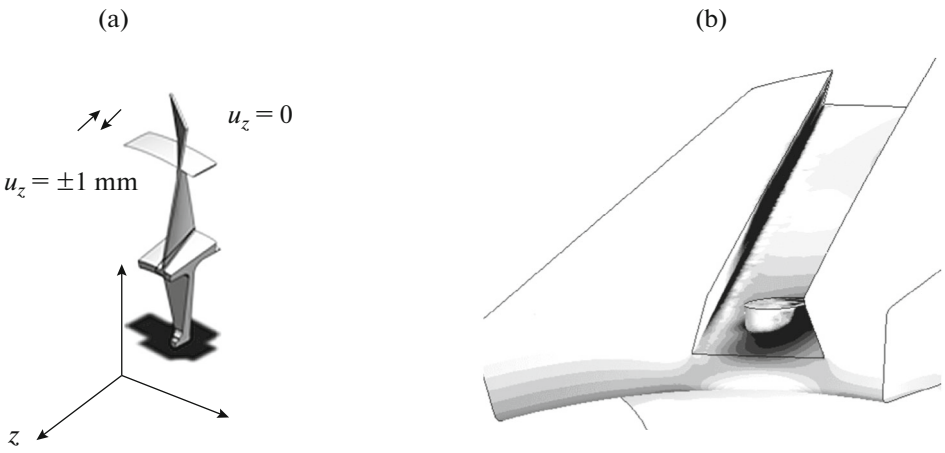

Fig. 5. (a) The scheme of the high-frequency cycle. (b) The greatest principal stress.

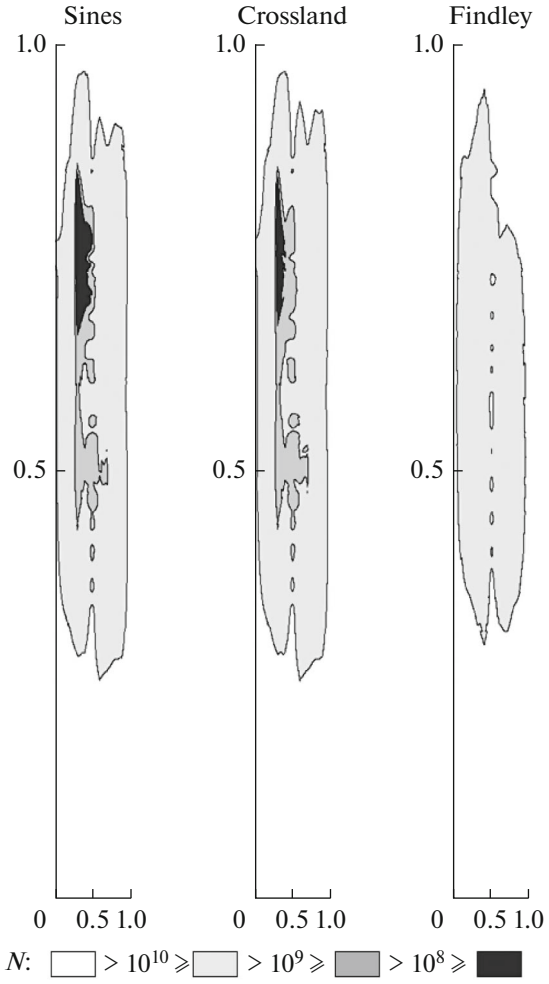

Fig. 6. The durability distribution for VHCF.

4.3. Durability Estimates According to the VHCF Criteria

In Fig. 6, we display the computed values of the number cycles to fracture N in vicinity of the left-hand angle of the contact junction between the disk and blade (in the zones of maximal stress concentration);

this is done for the three selected generalized VHCF criteria (Sines, Crossland, and Findley) with respect to the stressed state.

Although the level of stress amplitudes in the cycle is relatively low, we see from the computations that zones of possible fatigue fracture arise in this case as well. They are located at the back of the left corner of the groove, i.e., at about the same place as in the case of the flight loading cycles. Fatigue fracture zones arise at the number N on the order of 10^9–10^{10}, which means about 50000 hours of the real exploitation (we take the cycle period of 0.02 s for the selected oscillation frequency); this value is achievable in practice. Those estimates are quite approximate, but they show the possibility of a fatigue fracture (in the specified zones of the compressor disk) according to both mechanisms: LCF (the flight loading cycle) and VHCF (high-frequency low-amplitude vibrations of the construction elements). The mutual action of those mechanisms might be even more dangerous because they take place in closely located zones and in close real-time scales.

5. CONCLUSIONS

A comparative numerical analysis and durability estimates for the GTE compressor disk are provided for two alternative mechanisms (LCF and VHCF) of the fatigue fracture. The computations show that fatigue fracture zones for LCF and VHCF are closely located and their real-time durability estimates are close to each other.

ACKNOWLEDGMENTS

This study was supported in part by the Russian Foundation for Basic Research, project no. 15-08-02392.

REFERENCES

1. A. A. Shanyavskii, *Modeling of Metal Fatigue Fracture* (Monografiya, Ufa, 2007) [in Russian].
2. N. G. Burago, A. B. Zhuravlev, and I. S. Nikitin, "Models of multiaxial fatigue fracture and service life estimation of structural elements," Mech. Solids **46**, 828–838 (2011).
3. M. A. Meggiolaro, A. C. Miranda, and J. de Castro, "Comparison among fatigue life prediction methods and stress-strain models under multiaxial loading," in *Proceedings of the 19th International Congress of Mechanical Engineering COBEM 2007, Brasilia, DF, Brazil, Nov. 5–9, 2007.*
4. D. F. Socie and G. B. Marquis, *Multiaxial Fatigue* (Society of Automotive Engineers, Warrendale, PA, 2000), pp. 129–169.
5. N. Shamsaei, M. Gladskyi, K. Panasovskyi, S. Shukaev, and A. Fatemi, "Multiaxial fatigue of titanium including step loading and path alternation and sequence affects," Int. J. Fatigue **32**, 1862–1874 (2010).
6. J. Lemaitre and J. L. Chaboche, *Mechanics of Solid Materials* (Cambridge Univ. Press, Cambridge, 1994).
7. J. L. Chaboche and P. M. Lesne, "Non-linear continuous fatigue damage model," Fatigue Fract. Eng. Mater. Struct. **11**, 1–17 (1988).
8. A. K. Marmi, A. M. Habraken, and L. Duchene, "Multiaxial fatigue damage modeling at macro scale of Ti6Al4V alloy," Int. J. Fatigue **31**, 2031–2040 (2009).
9. I. V. Papadopoulos, P. Davoli, C. Goria, M. Filippini, and A. Bernasconi, "A comparative study of multiaxial high-cycle fatigue criteria for metals," Int. J. Fatigue **19**, 219–235 (1997).
10. Ying-Yu Wang and Wei-Xing Yao, "Evaluation and comparison of several multiaxial fatigue criteria," Int. J. Fatigue **26**, 17–25 (2004).
11. G. Sines, *Behavior of Metals under Complex Static and Alternating Stresses. Metal Fatigue* (McGraw-Hill, New York, 1959), pp. 145–169.
12. B. Crossland, "Effect of large hydrostatic pressures on torsional fatigue strength of an alloy steel," in *Proceedings of the International Conference on Fatigue of Metals* (London, 1956), pp. 138–149.
13. W. N. Findley, "A theory for the effect of mean stress on fatigue of metals under combined torsion and axial load or bending," J. Eng. Ind., 301–306 (1959).
14. C. Bathias and P. C. Paris, *Gigacycle Fatigue in Mechanical Practice* (Marcel Dekker, New York, 2005).
15. N. G. Burago, A. B. Zhuravlev, and I. S. Nikitin, "Stress state analysis of gas turbine engine contact system "disc-blades"," Vychisl. Mekh. Splosh. Sred **4** (2), 5–16 (2011).

16. V. Bonnand, J. L. Chaboche, H. Cherouali, P. Kanoute, E. Ostoja-Kuczynski, and F. Vogel, "Investigation of multiaxial fatigue in the prospect of turbine disc applications. Part II: Fatigue criteria analysis and formulation of a new combined one," in *Proceedings of the 9th International Conference of Multiaxial Fatigue and Fracture ICMFF9, Parma, Italy, 2010*, pp. 691–698.

17. N. G. Burago, A. B. Zhuravlev, and I. S. Nikitin, "Very-high-cycle fatigue fracture of titanium compressor disks," Vestn. Perm. Nats. Politekh. Univ., Mekh., No. 1, 52–67 (2013).

18. A. M. Mkhitaryan, *Aerodynamics* (Mashinostroenie, Moscow, 1976; PN, New York, 1972).

19. N. E. Kochin, I. A. Kibel', and N. V. Roze, *Theoretical Hydromechanics* (Fizmatgiz, Moscow, 1963; Wiley, New York, 1964), Part 1.

Translated by A. Muravnik